FEBS Letters 589 (2015) 967–973

journal homepage: www.FEBSLetters.org

Packing defects functionalize soluble proteins

Ariel Fernández *

Argentine Institute of Mathematics (I. A. M.), National Research Council (CONICET), Buenos Aires 1083, Argentina

ARTICLE INFO

Article history:
Received 29 December 2014
Revised 22 February 2015
Accepted 3 March 2015
Available online 13 March 2015

Edited by A. Valencia

Keywords:
Soluble protein
Structural biology
Molecular biophysics
Packing defect
Enzyme catalysis
Catalytic stimulation

ABSTRACT

This work explores the participation of protein packing defects, the so-called *dehydrons*, in biochemical events. We delineate the enabling role of dehydrons as activators of nucleophilic groups. This activation results from the induction of chemical basicity in interfacial water molecules, promoting deprotonation of adjacent nucleophiles. Through multiple steering molecular dynamics with pulling along the proton-displacement coordinate, we show that nucleophilic groups are functionally enabled by nearby dehydrons that promote proton transference. The computations are validated against experimentally determined pKa decreases at functional sites and biochemical probes of deregulated catalytic activity arising from dehydron-generating mutations.

1. Introduction

Dehydrons are packing defects in soluble proteins known to promote protein associations [1] and have been conjectured to induce chemical reactivity in interfacial water [2]. Dehydrons are solvent-exposed backbone hydrogen bonds and, in large concentration on the protein surface, can cause structural disruption by enabling backbone hydration. Thus, dehydrons introduce structure-destabilizing nanoscale cavities on the protein surface. These cavities create interfacial tension since backbone-solvating water under nanoscale confinement is deprived of hydrogen-bonding possibilities [3]. The interfacial tension caused by dehydrons is released upon protein associations that in effect displace the restricted interfacial water, turning dehydrons into promoters of protein interactions [3]. It has been further conjectured that water molecules enveloping dehydrons, thereby restricted in hydrogen-bond coordination, may act effectively as proton acceptors [2]. This chemical behavior appears to arise from a non-Debye polarization-induced negative charge arising as nanoscale confinement hampers the alignment of water dipoles with the electric field [2].

In this work we unravel the mechanism of functional enablement promoted by dehydrons in their role as inducers of chemical basicity of the aqueous interface. To that effect, we investigate the chemical event of proton transference prompted by water molecules at dehydron interfaces. Specifically, we compute the shifts towards lower values in pKa [4] of groups functionalized through dehydron-promoted deprotonation. To assess this activity we consider chemically active dehydrons in the proximity of the functional site, i.e. those for which the water oxygen in the dehydron cavity is within 6 Å of the α-carbon of the functional residue. The method of choice to investigate the chemical event of dehydron-induced proton transference is multiple steering molecular dynamics computation [5]. The nucleophilic group and nearby proton-receptive water molecule at the dehydron interface are treated within a quantum mechanical (QM) scheme while the rest of the molecule and explicit solvent are treated using a classical molecular mechanics (MM) package, in accord with a QM–MM hybrid approach [6,7]. The results are validated against experimentally determined pKa shifts [4] and functional studies of constitutively active mutant enzymes [8] whose aberrant deregulation is shown to arise from the creation of dehydrons not present in the wild type.

The study cases are selected so that the dehydron-promoted lowering of pKa value is significant and cannot be properly captured by current estimators of pKa shift. The latter are typically based on an empirical evaluation of pairwise interactions within a protein environment that favors a particular ionization state. Such estimators do not incorporate the unique electrostatic effects of structural or confined interfacial water molecules [2] into the empirical environmental field [4].

Author contributions: Ariel Fernandez conceived the idea, planned the work, performed the research, generated the data and wrote the paper.

* Fax: +54 11 4954 6782.
E-mail address: ariel@afinnovation.com

http://dx.doi.org/10.1016/j.febslet.2015.03.002

2. Materials and methods

To determine the functional stimulation caused by dehydrons, we compute the pKa decrease for nucleophilic side-chain groups with dehydrons in their proximity relative to the free residue in solution. As usual, the pKa shift, ΔpKa, estimates the difference in free energy increment, $\Delta\Delta G/RT = [\Delta G(p) - \Delta G(w)]/RT$, of the proton abstraction process in the protein environment (ΔG(p)) relative to the bulk aqueous environment (ΔG(w)). The results are contrasted against experimental data on ΔpKa. The free energy computation follows the multiple steering ansatz [5], where the molecular dynamics (MD) trajectories are generated by treating classically all groups except for those implicated in the chemical step of proton transference. The latter are treated in the quantum-mechanics (QM) density functional theory (DFT) setting [6]. The QM treatment is thus restricted to the side chain of the catalytic residues containing the weak-acid pro-nucleophilic group and to the reactive dehydron-associated water molecule. The reactive water molecule is defined as having its oxygen within 2.5 Å of the transitional proton that is initially covalently attached to a heavy atom (O, S or N) in the pro-nucleophilic group. The latter is generically denoted AH (or AH^+) and the neighboring distance cutoff is set so that the covalent bond A–H (or $[A-H]^+$ if protonation bestows charge) turns into hydrogen bond in the deprotonated state $A^-\cdots H(H_2O)^+$ (or $A\cdots H(H_2O)^+$) that results as the proton is transferred to the nearby dehydron-functionalized water molecule.

We denote by X the proton transference coordinate indicating the distance of the proton to the heavy atom initially covalently attached to it in the weakly acidic pro-nucleophile. Thus, $X(t = 0) = X_0$ is the bond length corresponding to covalent bonding to the heavy atom in the nucleophile and $X–X_0$ measures departure from covalent bond length. We denote by $\boldsymbol{R}$ the structural-coordinate vector for protein chain and water. In accord with the Jarzynski identity [5], $\Delta G(p)/RT = -\log\langle\exp[-W(X, \boldsymbol{R}(X))/RT]\rangle$, where the average $\langle\exp[-W(X, \boldsymbol{R}(X)]\rangle$ (W = computed work) extends over all trajectories $\boldsymbol{R}(X(t))$ with structural conformations steered by the pulling $X = X_0 \rightarrow X = X_0 + v(t_f)$ at constant speed v along the harmonic proton-transference linear coordinate. The pathway ensemble $\{\boldsymbol{R}(X(t))\}$, is generated by choosing initial conformations $\boldsymbol{R_0} = \boldsymbol{R}(X_0)$ within an isothermal/isobaric equilibrated ensemble (T = 298 K). This ensemble realizes the condition $X = X_0$ and is generated by a set of 20 classical thermalization trajectories, each lasting 1 ns, with the PDB-reported structure fixed at the initial condition. The trajectory multiplicity arising from X-pulling is provided by the conformational dispersion in the initial ensemble $\{\boldsymbol{R_0} = \boldsymbol{R}(X_0)\}$, with each initial conformation responding differently to the X-pulling.

The QM region is treated using flexible basis sets of linear combinations of finite atomic orbitals in a real space grid optimized to N-scaling. The basis functions enable the matching of the radial wave function to the core region described by pseudopotentials by using pseudoatomic orbitals (PAOs) [9]. Split valence bases are generated by combining numerical Gaussian orbitals with the minimal basis described. The nuclei and core electrons are represented by norm-conserving pseudopotentials to avoid the computation of core states, a procedure that smoothens out the valence charge density in accord with grid requirements. Within the non-local pseudopotential approximation, a Kohn–Sham Hamiltonian is adopted incorporating the Hartree and exchange–correlation potentials, and a pseudopotential with additive contributions to account for local effects, long-range interactions and operation on valence electrons [10]. Calculations are performed on contracted Gaussian basis sets of double-zeta valence polarized (DZVP) quality (pseudoatomic orbital energy shift = 30 meV, grid cutoff = 135 Ry) [11].

The MM region is treated as detailed in [3,12], where torsional degrees of freedom of backbone and side chains are coarse grained modulo basins of attraction in the potential energy surface in accord with Ramachandran (energetically allowed) regions in local conformation space. Interfacial water dipoles confined to dehydron cavities are subject to a torque resulting from the hindrance to alignment with the electrostatic field [3]. To equilibrate the PDB-reported structures with the solvent, we generated MD trajectories driven by the coarse-grained stochastic process, incorporating the potential energy associated with solvent orientation steering as the reversible work needed to align polarization-induced dipoles due to interfacial water confinement with the Debye electrostatic field [12]. To cover relevant timescales (~10 ns), the dynamics are entrained by the coarser "protodynamics", where the backbone (ϕ, ψ) dihedral torsions are specified "modulo basins of attraction" in the potential energy surface. Coarse moves are defined as transitions between basins of attraction (R-basins) in the Ramachandran torsional (ϕ, ψ)-map for each residue. Thus, each residue is assigned an R-basin after a coarse move, and the coarse state of the chain becomes a conformational ensemble, with each conformation generated by selecting individual (ϕ, ψ)-coordinates within the assigned R-basins [3].

The hybrid Hamiltonian incorporated includes QM-MM coupling comprised of three contributions: (1) electrostatic interaction between electrons and classical charges, (2) electrostatic interactions between nuclei in the QM subsystem and the classical point charges, and (3) a Lennard–Jones 6–12 potential to account for the van der Waals interactions between the atoms in MM and QM regions constructed using the force-field parametrization of Wang et al. [13]. The forces on the QM nuclei are obtained by taking the gradient with respect to atomic positions, and include derivation of the QM–MM coupling energy. The implementation details and description of the package adopted to conduct QM/MM hybrid computations is presented in the Supplementary Data.

3. Results

The quasi-equilibrated work plots harvested in the free-energy computation associated with the dehydron-induced proton transfer event do not portend and are not required to reproduce the actual kinetics, which occurs on much faster timescales. The work performed by the system to reach the point $X = X_0 + vt$ along the proton transference coordinate is shown in Fig. 1a for the imidazole >NH group in His149 of *xylanase* (PDB.1XNB) for ten realizations, $\boldsymbol{R_0} = \boldsymbol{R}(X_0)$ of the initial condition $X = X_0$ with harmonic force constant 48 kJ/mol. The thin lines indicate the work performed on the system at each point $X = X_0 + vt$ along the X-pulling steering trajectory with v = 0.2 Å/ns and t_f = 6 ns. The thick lines correspond to slower pulling at v = 0.1 Å/ns with t_f = 12 ns. The work histories for proton transference from imidazole in a free His amino acid in bulk water are shown in Fig. 1b. The dehydronic environment of His149 in xylanase structure is displayed in Fig. 1c. The His149 residue is required to be deprotonated in its structure-stabilizing function exerted by hydrogen bonding Ser130, internal water and by engaging in a putative aromatic–aromatic interaction with Tyr105 [14]. The case illustrated represents a dramatic pKa shift, with ΔpKa < –3.8, from the pKa value ~6.1 for free protonated imidazole in bulk water to <2.3 in the xylanase environment [4]. The dehydron-functionalized water molecule around vicinal dehydron Ser100-Gly103 in the initial conformation $\boldsymbol{R_0} = \boldsymbol{R}(X_0)$ shown in Fig. 1d serves as acceptor of the imidazole proton in His149, with the associated chemical event schematized in Fig. 1e. Other conformations use the environment around the other vicinal dehydron Thr145-Asn148 for proton acceptance. A computed value of ΔpKa = –3.77 is obtained for 20 trajectories

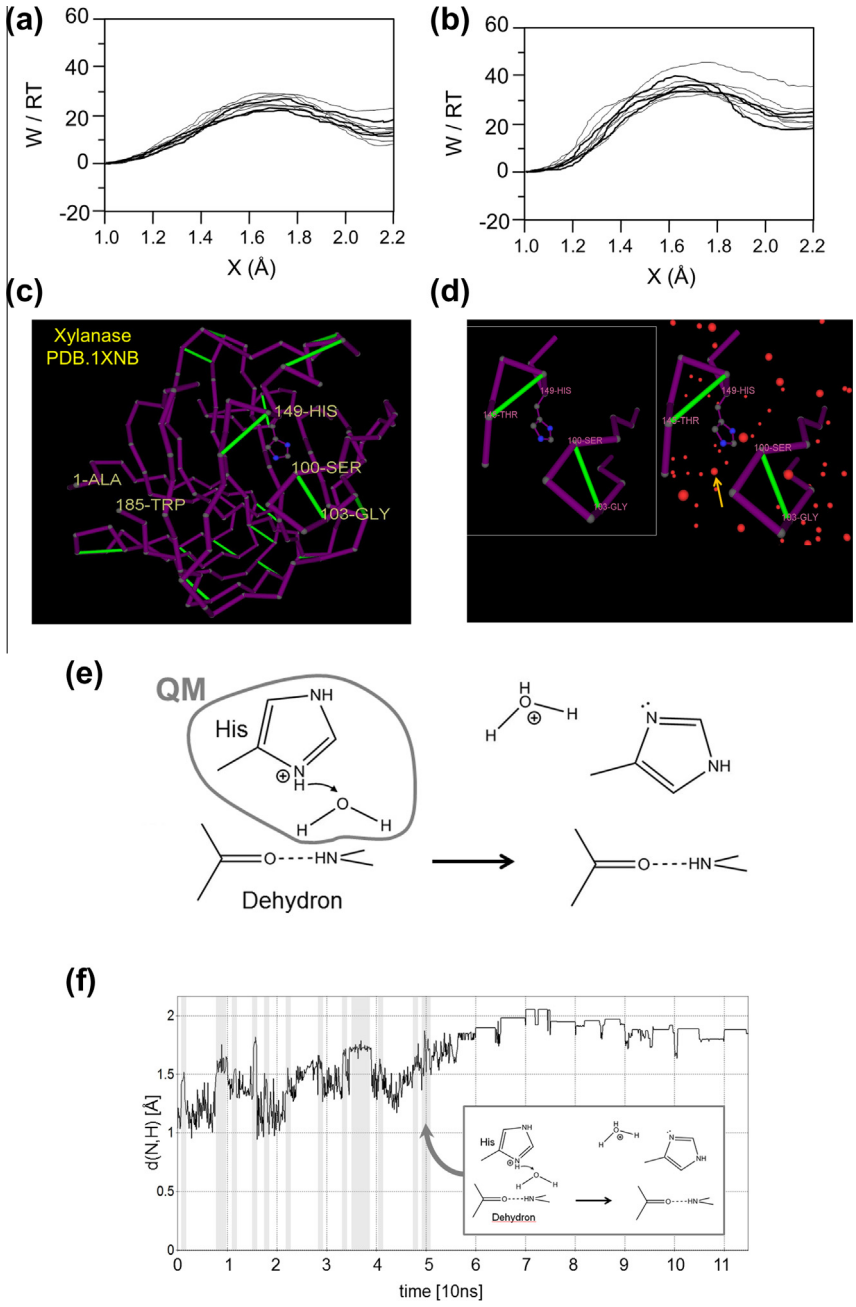

Fig. 1. (a) Work performed by the xylanase–solvent system to reach the point $X = X_0 + vt$ along the proton transference coordinate X for the imidazole >NH group in His149. The histories displayed correspond to 10 initial conformations satisfying $X = X_0$. Thin lines were obtained at pulling speed $v = 0.2$ Å/ns and total pulling time $t_f = 6$ ns. The thick lines correspond to $v = 0.1$ Å/ns, with $t_f = 12$ ns. (b) Work associated with proton transference from a free His imidazole in bulk water, with pulling speeds along the X coordinate represented as in (a). (c) Dehydron pattern of an equilibrated xylanase structure at $X = X_0$, with dehydrons Ser100-Gly103 and Thr145-His149 flanking His 149 (side chain displayed). The backbone is schematically represented as virtual bonds joining α-carbons and dehydrons are displayed as sticks joining the non-adjacent α-carbons of the hydrogen bonded residues. (d) Dehydronic environment for His149 in xylanase at $X = X_0$ with the same structural representation as in (c). The oxygen atoms of interfacial water molecules are displayed and the interfacial water molecule with proton-accepting capability induced by dehydron Ser100-Gly103 is indicated by the arrow. (e) Chemical depiction of the proton transference event from histidine imidazole to the dehydron-functionalized water molecule, as monitored along coordinate X. (f) Unrestrained QM/MM computation capturing the spontaneous dehydron-induced deprotonation of the imidazole side-chain group in His149 from xylanase (PDB.1XNB). Deprotonation is monitored through the imidazole N–H distance along a 110 ns trajectory. The vicinity of an interfacial water molecule to the His149-functionalizing Ser100-Gly103 dehydron is marked by a distance between backbone carbonyl and water oxygen atoms <3.3 Å. The presence of the dehydron-vicinal water molecule at specific time periods is marked by gray bands. After eleven failed attempts, this dehydron-induced basic water promotes imidazole deprotonation at ~50 ns, a chemical event described in the inset.

generated by X-pulling at $v = 0.2$ Å/ns, while $\Delta pKa = -3.64$ is obtained by collecting 20 trajectories at slower velocity $v = 0.1$ Å/ns, with both pKa shifts in good agreement with the experimental measurement [4]. Since it does not incorporate the dehydron-induced basicity of the aqueous interface, a classical explicit-solvent thermodynamic computation (Supplementary Data) yields $\Delta pKa = -1.12$, barely reproducing the correct trend in pKa.

In control computational experiments, we address the question of whether the QM/MM computation may capture the *spontaneous* dehydron-induced deprotonation of the nucleophilic group

without introducing a "pulling" coordinate. Such computations are more costly than equilibration steered along a pre-determined reaction coordinate since they involve capturing a specific spontaneous chemical event within an unrestrained equilibration process. From the practical side, such computations do not yield the free energy change associated with the chemical event, which requires computing the work along manifold trajectories steered by a specified pulling coordinate [1]. A control QM/MM equilibration trajectory was performed for xylanase (PDB.1XNB) with QM treatment of side-chain imidazole group of His149 and dehydron-functionalized water molecule identified by a distance between backbone carbonyl and water oxygen atoms <3.3 Å. The perturbative elastic *X*-contribution to the Hamiltonian was removed and the computation was run for 110 ns with deprotonation monitored through the imidazole N–H distance. Strikingly, the water molecule vicinal to the His149-functionalizing Ser100-Gly103 dehydron had remarkably long residence times (∼1 to ∼4 ns), revealing the slow dynamic nature of the dehydron interface when the packing defect is also endowed with a chemical role. The basic interfacial water molecule may be regarded as temporarily intercalated between the carbonyl oxygen of the functionalizing Ser100-Gly103 dehydron and the His149-bonded labile imidazole proton. In this location, the dehydron-associated water molecule is capable of eventually triggering imidazole deprotonation and depart as hydronium, a spontaneous chemical event observed at 50 ns after eleven previous failed attempts (Fig. 1f). It should be noted that the dynamics of the chemically functional dehydron interface can only be properly captured when the steering perturbative term is removed from the QM/MM hybrid Hamiltonian.

A second computation of extreme pKa shifting, shown here to be due to dehydronic stimulation involves Asp70 in RNase H (PDB.2RN2), flanked by dehydrons Asn44-Glu48, Thr69-Val121, Lys122-Ala125 and His127-Glu131 (Fig. 2a). The carboxyl in Asp70 must remain highly nucleophilic since it is implicated in enzyme activation by ion coordination through lone electron-pair donation to Mn^{2+} [15]. In this case, the proton transference from the carboxyl group in Asp70 to proton-receptive vicinal water involves the water molecule associated with dehydron Asn44-Glu48 (Fig. 2b). The multiple steering QM–MM computation yields a shift $\Delta pKa = -1.32$ in coincidence with the experimental value [4] and in sharp contrast with other computations ($\Delta pKa = +0.30$ [4]) that ignored dehydronic effects. A classical explicit-solvent thermodynamic computation (Supplementary Data) yields $\Delta pKa = +0.91$, also failing to capture the correct trend in pKa, as it factors in the hindrance of proton migration as culprit for a relatively unfavorable deprotonation in the protein environment.

As in the previous study case, an unrestrained QM/MM computation run for 50 ns was performed to capture the *spontaneous* deprotonation of the carboxyl side-chain group in Asp70 induced by the Asn44-Glu48 dehydron in *RNase H*. Deprotonation is monitored through the carboxyl O–H distance (Fig. 2c). The presence of the dehydron-vicinal water molecule triggering Asp70 deprotonation is marked by the gray band. The higher success rate in the dehydron-induced deprotonation of aspartic compared to histidine (cf. Figs. 1f and 2c) is due to the far lower pKa of free carboxyl relative to imidazole (3.8 versus 6.1, approximately).

A third study case revealing dehydronic effects in group functionalization is furnished by the pKa shift due to protein environment at His114 in RNase H. This residue in its deprotonated state is implicated in structural stabilization [16]. A shift $\Delta pKa \approx -1.63$ is calculated by defining the reaction coordinate *X* through the imidazole deprotonation induced by dehydron Cys63-Gln115 (Fig. 2d). The pKa shift obtained is identical to the experimental value and at a variance with other computations ($\Delta pKa = +1.20$ [4]) that do not incorporate dehydronic effects. On the other hand, the classical explicit-solvent thermodynamic computation (Supplementary Data) yields $\Delta pKa = -0.34$, barely capturing the correct trend in pKa for this relatively exposed residue. As in the previous cases, an unrestrained QM/MM 100 ns run reveals the spontaneous dehydron-induced imidazole deprotonation that in this case occurs at ∼45 ns.

Finally, residue Glu13 on chain B of human insulin is known to play a crucial role in oligomerization [17] and association with the islet amyloid polypeptide (IAPP) through an intermolecular salt bridge [18]. These structural roles require a functionalization evidenced in the shift $\Delta pKa = -1.90$. Current pKa computations that do not incorporate the dehydron influence yield the incorrect value $\Delta pKa = -0.30$ [4]. The shift is correctly estimated by taking into account the enabling role of vicinal dehydron Ala14-Val18 on chain B (Fig. 2e). The chemical event of deprotonation of Glu13 is captured by implicating the interfacial water molecule (marked by an arrow in Fig. 2e) turned into a proton acceptor by dehydron Ala14-Val18. The multiple steering MD computation pulling along the proton transference coordinate yields $\Delta pKa = -1.81$ in satisfactory agreement with experiment [4]. An explicit-solvent thermodynamic computation (Supplementary Data) yields $\Delta pKa = -0.78$, a figure relatively far from the experimental value but at least indicative of the trend in the protein environment. On the other hand, an unrestrained QM/MM run for 50 ns (computational details in Supplementary Data) reveals a spontaneous dehydron-induced carboxyl deprotonation at ∼8 ns.

The biochemical consequences of dehydron-stimulated catalytic activity are probed by examining the effects of oncogenic mutations yielding constitutively active enzymes. We focus on cancer-related kinases altered by dehydron-generating mutation. As it is known, kinases get phosphorylated by performing a nucleophilic attack on the terminal ATP phosphoester linkage. Thus, our working hypothesis is that the nucleophilicity of the active side chain is enhanced in the mutant variant provided the mutation generates stimulating dehydrons nearby. With this rationale in mind, we investigate the oncogenic mutation D816V (Asp816Val) in the c-Kit kinase, found in mastocytosis [19] and other tumors, and known to induce a transforming capacity in c-Kit by turning it constitutively active [8]. The mutation D816V occurs in a floppy region of the kinase known as activation loop. A set of five 1.1 μs MD trajectories were generated on the wild-type kinase and on the D816V substitution by equilibrating the PDB-reported conformation 1T46 following the coarse-graining protocol previously described [3,12]. The hydrophobic replacement resulting from mutation D816V promotes water exclusion (wrapping) at backbone hydrogen bond Gly812-Arg815 that is retained as a dehydron (Fig. 3a). This hydrogen bond is disrupted in the wild type due to backbone hydration, as the activation loop becomes more solubilized by the presence of polar residue Asp816 (Fig. 3b). In turn, the presence of the Gly812-Arg815 dehydron in the vicinity of the phosphorylation site Tyr823 in the c-Kit mutant, lowers significantly the pKa of the phenolic hydroxyl in Tyr823, as shown in the structural display for the mutant (Fig. 3c). The enhanced nucleophilicity of Tyr823 is the resultant of the proton acceptor activity of interfacial water (Fig. 3d) promoted by mutation-induced dehydron Gly812-Arg815. Multiple steering MD computations yield $\Delta pKa = -2.7$ as the mutation-generated dehydron functionalizes its adjacent water molecule into a proton acceptor (Fig. 3c) for the phenolic hydroxyl proton of Tyr823 (Fig. 3d). This enhancement in the nucleophilicity of the Tyr823 also enhances significantly its phosphorylation since the latter is contingent on nucleophilic attack on the ATP phosphoester linkage. Consequently, the mutation D816V turns the kinase constitutively active. It is now known that Tyr823 phosphorylation is essential to recruit anti-apoptotic pathways that bestow the transforming

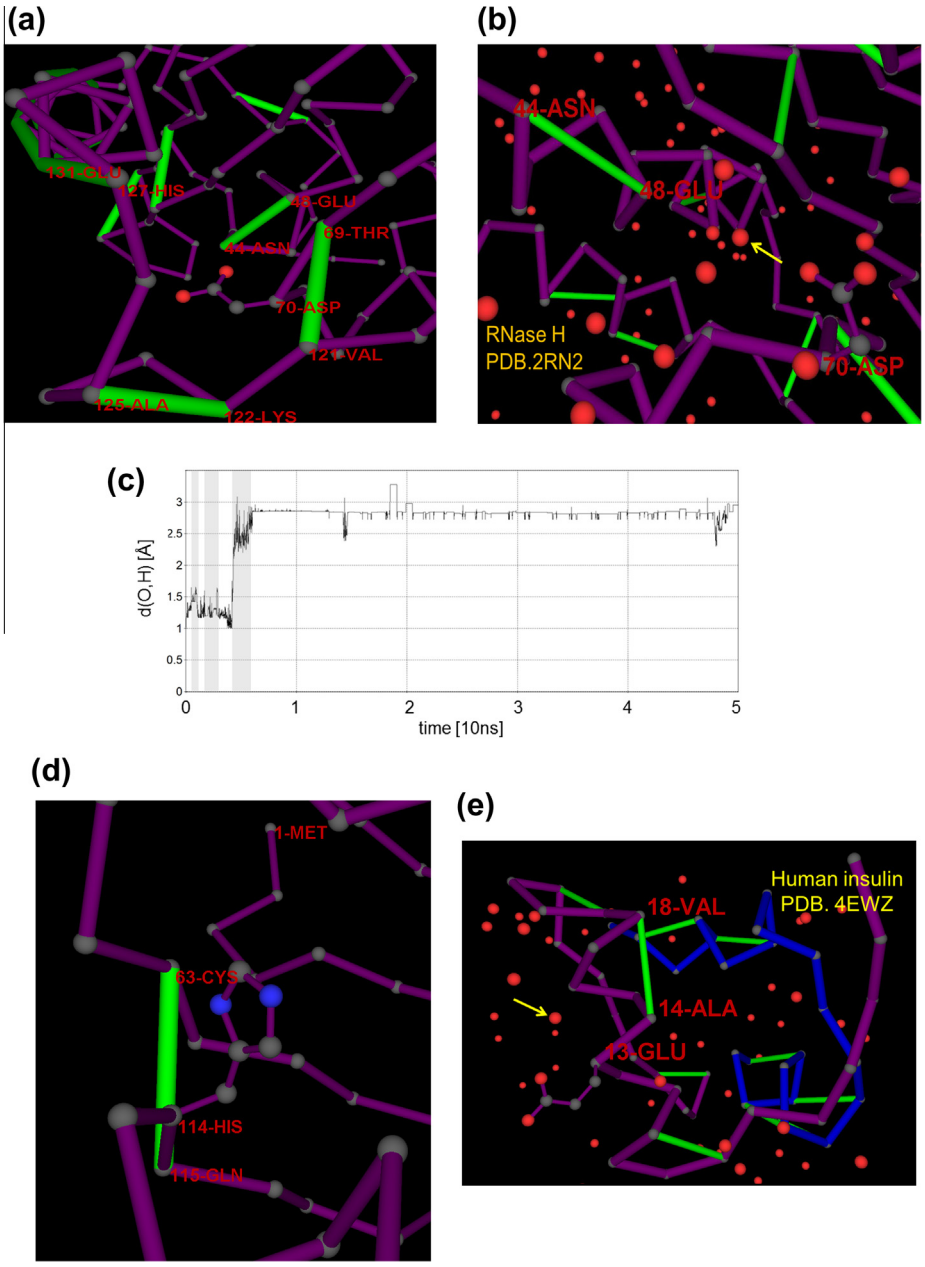

Fig. 2. (a) Dehydronic environment for Asp70 in RNase H. The surrounding dehydrons are Asn44-Glu48, Thr69-Val121, Lys122-Ala125 and His127-Glu131. The representation convention is as described for (c). (b) Interfacial water around Asp70 in RNase H. The proton-receptive vicinal water marked by the arrow is associated with dehydron Asn44-Glu48 and promotes the proton transference from carboxyl group in Asp70. (c) Unrestrained QM/MM computation capturing the spontaneous dehydron-induced deprotonation of the carboxyl side-chain group in Asp70 from RNase H (PDB.2RN2). Deprotonation is monitored through the carboxyl O–H distance along a 50 ns trajectory. The presence of the dehydron-vicinal water molecule eventually triggering Asp70 deprotonation is marked by gray bands. (d) Dehydron environment for His114 in RNase H with imidazole deprotonation induced by dehydron Cys63-Gln115. (e) Dehydronic environment for Glu13 in chain B of human insulin. The water molecule marked by the arrow hydrates dehydron Ala14-Val18 and behaves as a proton acceptor for the side chain of Glu13.

capability to c-Kit, leading to significantly longer tumor lifetime [8]. Thus, the oncogenic nature of the mutation may be now traced to its physico-chemical roots.

The D816V mutation-based enhancement of the Tyr823 nucleophilicity is completely missed in a classical all-atom explicit solvent thermodynamic computation (details in Supplementary Data). This method yields $\Delta pKa = +0.87$, as it accounts for the hindrance of Tyr823 deprotonation that results from the increase in local hydrophobicity brought about by the D816V substitution. Although the result is incompatible with the experimental facts, *prima facie* it makes intuitive sense, as the lower dielectric environment created by the polar-to-non-polar D816V substitution would significantly raise the self-energy of the leaving hydronium. The paradox may be resolved by noting that the D816V substitution enhances the backbone desolvation thereby inducing the formation of the Gly812-Arg815 dehydron. The dehydron-associated interfacial water becomes basic due to its frustration in hydrogen bonding opportunities [2,3], enabling Tyr823 deprotonation. Furthermore, the dehydron introduces a breakdown in the Debye dielectric picture [20], as its nanoscale confinement of interfacial water generates a polarization contribution that does not align with the protein electrostatic field, so the concept of

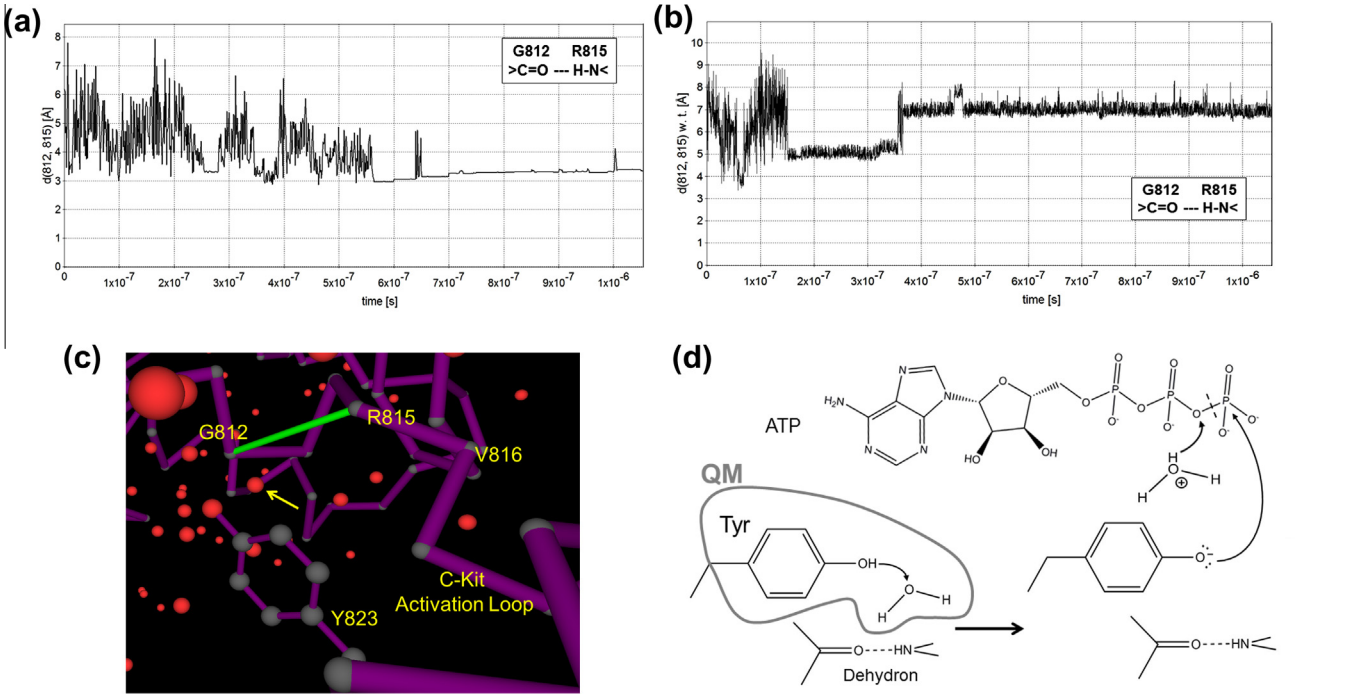

Fig. 3. (a) Time-dependent O–N distance between backbone carbonyl of Gly812 and backbone amide of Arg815 in the activation loop of c-Kit D816V mutant along a typical 1.1 μs MD trajectory generated as described in main text (details in Refs. [12,13]). The initial torsional state is the PDB-reported in entry 1T46. A stable Gly812-Arg815 backbone hydrogen bond emerges after 0.65 ± 0.20 μs in all 5 trajectories generated. (b) Time-dependent backbone O–N distance between Gly812 and Arg815 in wild type c-Kit along a typical 1.1 μs MD trajectory. No stable backbone hydrogen bond is observed in any trajectory. (c) Snapshot of the activation loop of mutant D816V after 1.1 μs equilibration (cf. (a)) displaying dehydron Gly812-Arg815. The interfacial water molecule implicated in proton transference and functionalization of Tyr823 is marked by the arrow. (d) Chemical event of dehydron-based functionalization of a Tyr side chain as required for transesterification reaction with ATP.

"local permittivity coefficient" becomes blurry at best. All in all, the experimental facts seem consistent with a non-Debye picture in which the mutation-induced dehydron becomes an enabler and stimulator of catalytic activity that in this case results from Tyr823 nucleophilicity.

4. Discussion

In this study, we mechanistically explored and validated the previously established conjecture that protein packing defects - the so-called *dehydrons* – participate as quasi-reactants in biochemical events [2]. We focused on protein functions involving nucleophiles activated through deprotonation promoted by nearby dehydrons. Through molecular dynamics steered by pulling along the proton-transference coordinate, we unraveled a general mechanism for dehydron-based functionalization. The results were validated against experimentally determined pKa shifts and biochemical probes of deregulated catalytic activity arising from dehydron-generating mutations. Thus, the mechanistic/structural underpinnings of dehydron-based protein functionalization are established.

Acknowledgments

The author is indebted to his former Rice University Ph. D. student Dr. Jianping Chen (Shenzhen, China) for the implementation of the QM/MM multiple steering calculations on the Rice Computational Research Cluster. Enlightening conversations with Prof. Ridgway Scott (University of Chicago) are gratefully acknowledged.

Appendix A. Supplementary data

Supplementary data associated with this article can be found, in the online version, at http://dx.doi.org/10.1016/j.febslet.2015.03.002.

References

[1] Fernández, A. and Crespo, A. (2008) Protein wrapping: a molecular marker for association, aggregation and drug design. Chem. Soc. Rev. 37, 2373–2382, http://dx.doi.org/10.1039/B804150B.
[2] Fernández, A. (2014) Communication: chemical functionality of interfacial water enveloping nanoscale structural defects in proteins. J. Chem. Phys. 140, 221102, http://dx.doi.org/10.1063/1.4882895.
[3] Fernández, A. (2013) The principle of minimal episteric distortion of the water matrix and its steering role in protein folding. J. Chem. Phys. 139, 085101, http://dx.doi.org/10.1063/1.4818874.
[4] Li, H., Robertson, A.D. and Jensen, J.H. (2005) Very fast empirical prediction and rationalization of protein pKa values. Proteins Struct. Funct. Bioinform. 61, 704–721, http://dx.doi.org/10.1002/prot.20660.
[5] Jarzynski, C. (1997) Nonequilibrium equality for free energy differences. Phys. Rev. Lett. 78, 2690–2693, http://dx.doi.org/10.1103/PhysRevLett.78.2690.
[6] van der Kamp, M.W. and Mulholland, A.J. (2013) Combined quantum mechanics/molecular mechanics (QM/MM) methods in computational enzymology. Biochemistry (ACS) 52, 2708–2728, http://dx.doi.org/10.1021/bi400215w.
[7] Senn, H.M. and Thiel, W. (2009) QM/MM methods for biomolecular systems. Angew. Chem. Int. Ed. 48, 1198–1229, http://dx.doi.org/10.1002/anie.200802019.
[8] Agarwal, S., Kazi, J.U. and Ronnstrand, L. (2013) Phosphorylation of the activation loop tyrosine 823 in c-Kit is crucial for cell survival and proliferation. J. Biol. Chem. 288, 22460–22468, http://dx.doi.org/10.1074/jbc.M113.474072.
[9] Sankey, O.F. and Niklewski, D.J. (1989) Ab initio multicenter tight-binding model for molecular-dynamics simulations and other applications in covalent systems. Phys. Rev. B 40, 3979–3995, http://dx.doi.org/10.1103/PhysRevB.40.3979.
[10] Kleinman, L. and Bylander, D.M. (1982) Efficacious form for model pseudopotentials. Phys. Rev. Lett. 48, 1425–1428, http://dx.doi.org/10.1103/PhysRevLett. 48.1425.
[11] Chiodo, S., Russo, N. and Sicilia, E. (2005) Newly developed basis sets for density functional calculations. J. Comput. Chem. 26, 175–184, http://dx.doi.org/10.1002/jcc.20144.
[12] Fernández, A. (2014) Fast track communication: water promotes the sealing of nanoscale packing defects in folding proteins. J. Phys. Cond. Matter 26, 202101, http://dx.doi.org/10.1088/0953-8984/26/20/202101.
[13] Wang, J., Cieplak, P. and Kollman, P.A. (2000) How well does a restrained electrostatic potential (RESP) model perform in calculating conformational energies of organic and biological molecules? J. Comput. Chem. 21, 1049–

1074, http://dx.doi.org/10.1002/1096-987X(200009)21:12<1049::AID-JCC3>3.0.CO;2-F.
[14] Plesniak, L.A., Connelly, G.P., Wakarchuk, W.W. and McIntosh, L.P. (1996) Characterization of a buried neutral histidine residue in *Bacillus circulans* xylanase: NMR assignments, pH titration, and hydrogen exchange. Protein Sci. 5, 2319–2328, http://dx.doi.org/10.1002/pro.5560051118.
[15] Goedken, E.R. and Marqusee, S. (2001) Co-crystal of *Escherichia coli* RNase HI with Mn2+ ions reveals two divalent metals bound in the active site. J. Biol. Chem. 276, 7266–7271, http://dx.doi.org/10.1074/jbc.M009626200.
[16] Kanaya, S., Katayanagi, K., Morikawa, K., Inoue, H., Ohtsuka, E. and Ikehara, M. (1991) Effect of mutagenesis at each of five histidine residues on enzymatic activity and stability of ribonuclease H from *Escherichia coli*. Eur. J. Biochem. 198, 437–440, http://dx.doi.org/10.1111/j.1432-1033.1991.tb16033.x.
[17] Bentley, G.A., Brange, J., Derewenda, Z., Dodson, E.J., Dodson, G.G., Markussen, J., Wilkinson, A.J. and Wollmer, A. (1992) Role of B13 Glu in insulin assembly. The hexamer structure of recombinant mutant (B13 Glu → Gln) insulin. J. Mol. Biol. 228, 1163–1176, http://dx.doi.org/10.1016/0022-2836(92)90323-C.
[18] Wei, L., Jiang, P., Yau, Y.H., Summer, H., Shocha, S.G., Mu, Y. and Pervushin, K. (2009) Residual structure in islet amyloid polypeptide mediates its interactions with soluble insulin. Biochemistry (ACS) 48, 2368–2376, http://dx.doi.org/10.1021/bi802097b.
[19] Piao, X. and Bernstein, A. (1996) A point mutation in the catalytic domain of c-kit induces growth factor independence, tumorigenicity, and differentiation of mast cells. Blood 87, 3117–3123.
[20] Fernández, Stigliano A. (2013) Breakdown of the Debye polarization ansatz at protein–water interfaces. J. Chem. Phys. 138, 225103, http://dx.doi.org/10.1063/1.4810867.